AD NUMBER

AD911780

LIMITATION CHANGES

TO:

Approved for public release; distribution is unlimited.

FROM:

Distribution authorized to U.S. Gov't. agencies only; Administrative/Operational Use; JUL 1973. Other requests shall be referred to Army Advanced Ballistic Missile Defense Agency, Huntsville, AL.

AUTHORITY

USASSC Itr, 21 Mar 1974

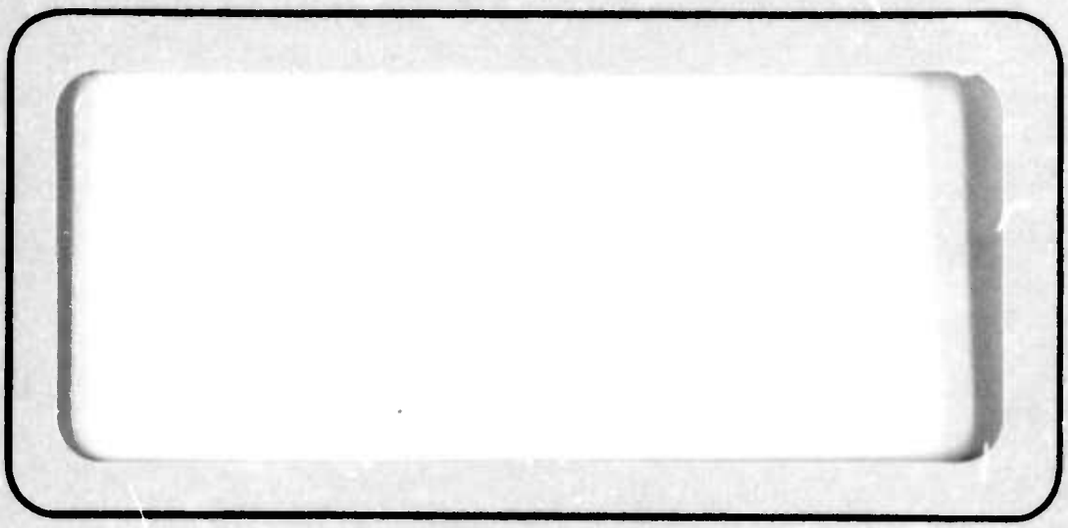

TRW
SYSTEMS GROUP
ONE SPACE PARK • REDONDO BEACH, CALIFORNIA

ROPE PROJECT

SEMI-ANNUAL TECHNICAL REPORT

18586-6051-RU-00

July 1973

Project Manager - J. T. Ohrenberger

This work was supported by ABMDA and the Advanced Research Projects Agency of the Department of Defense and was monitored by ABMDA under Contract No. DAHC60-71-C-0049 and ARPA Order 1953.

Th[redacted] spec[redacted] the U.S. Army Advanced Ballistic Missile Defense Agency, Huntsville Office, ATTN: [redacted], P. O. Box 1500, Huntsville, Alabama 35807.

RDMH-O

TRW
SYSTEMS GROUP

One Space Park • Redondo Beach, California 90278

CONTRIBUTORS

Section	Contributor
1.0	J. T. Ohrenberger
2.0	E. Baum

TABLE OF CONTENTS

ILLUSTRATIONS

1. TURBULENT BOUNDARY LAYER AND NEAR WAKE

1.1 Introduction

The major accomplishment of this task, to date, has been the successful implimentation of a turbulence modeling theory into the previous laminar near wake code. First results have been obtained, and will be presented here, corresponding to ABMDA-sponsored wind tunnel tests conducted at AEDC by Gran[1] on a 6 degree half angle adiabatic cone at Mach 7.5 and free-stream Reynolds number = 1.7×10^6, based on base diameter. These calculations represent the beginning of the portion of the analysis directed towards improving and verifying the implimented turbulence modeling theory for the wake problem. This is a crucial part of the analysis of the turbulent near wake, since the eventual goal of the present task is to apply the modeling to reentry vehicles under conditions in which no detailed flowfield and turbulence measurements have been made. Other planned tests of the theory will be subsequently discussed, but first an outline of the theory and a discussion of the new results will follow.

1.2 Description of Analysis

The near wake analysis begins with the calculation of the interacting boundary layer on the vehicle upstream boundary layer separation. The present theory was developed for vehicles with rounded, as opposed to sharp, aft corners, and the test model was also configured with an aft shoulder radius of 1/6 the base radius. Starting on the straight portion of the cone just upstream of the shoulder junction, it is possible to generate an infinitude of separation solutions where each solution corresponds to a different separation point on the shoulder, and hence, to a different separation pressure. The proper or unique separation solution depends upon the downstream behavior of the flow in the wake region. In the present formulation, a saddle point singularity exists in the wake neck downstream of the wake stagnation point, and the only acceptable wake solution is the solution which passes through the singularity. Solutions which lie on either side of the saddle point are referred to as either sink or source solutions and, as will be shown later, are characterized by non-wake-like behaviors. The wake solution begins at separation, and only a particular

separation solution will yield the wake solution which passes through the singularity; uniqueness of the separation and near wake flowfield solution is thereby obtained.

The wake neck saddle point, discussed above, is the well-known Crocco-Lees critical point and results from an analysis of viscous interaction flows based upon a parabolic description of the flow. In the present analysis of both the boundary layer and wake, the governing equations are written in a coordinate system consisting of streamlines and normals to streamlines. The governing equations contain the full inviscid terms and viscous terms associated with the cross-stream diffusion of momentum and energy. They are, therefore, parabolic, but are more than just boundary-layer-like in that both the streamwise and cross-stream pressure gradients are included. Thus, the expansion of the boundary layer into the wake and the compressions associated with the lip and wake shock waves can be calculated.

The mean flow and auxiliary equations are presented in References 2 and 3 for laminar flow. They differ from the equations solved here by the inclusion of cross-stream turbulent diffusion of momentum and energy, and by the addition of two differential equations which describe the turbulence. The turbulence modeling will be discussed subsequently in detail.

1.3 Turbulence Modeling

In the present theory, the non-homogeneous turbulence field is characterized at each point by two independent variables consisting of the turbulent kinetic energy, $e = (\overline{u'^2 + v'^2 + w'^2})/2$ and a lateral scale length of the turbulence, ℓ. To solve for these variables, two partial differential equations are written, each which represents a balance between the production, dissipation, diffusion, and convection of turbulent energy and its rate-of-dissipation. Because of the closure problems always encountered in the Reynolds description of turbulence, the terms appearing in the governing equations are models of the actual processes and are, therefore, approximate. However, reasonable success has been obtained by a number of investigators in the calculation of boundary layers and mixing layers and, consequently optimism exists for the near wake problem. A more rigorous and detailed

description of the turbulence which considers its true tensorial character, wherein correlations between all three components of velocity fluctuation as well as orthogonal integral scale lengths obtained from the various spectra are included, could also be applied in principle. However, this approach also suffers from the uncertainties of the closure assumptions, and the additional complexity of many more turbulence variables, constants to be determined, and equations to solve makes it too unwieldy for the near wake problem. The lumped or scalar representation of turbulence by two variables is the simplest representation which contains sufficient generality to be applicable to the near wake.

In addition to the two turbulence equations which must be solved along with the mean flow equations, the mean flow momentum and energy equations must be altered to contain turbulent diffusion. In the present theory, the Reynolds stress is represented by an eddy viscosity model such that $\overline{u'v'} = e^{1/2}\ell\ \partial U/\partial n$ where n is in a direction normal to the local mean flow streamlines. The diffusion flux terms for shear and heat transfer in the mean flow momentum and energy equations are written with both the laminar and turbulent components as

$$\tau_L - \rho\ \overline{u'v'} = \left(\mu + \rho\ e^{1/2}\ell\right)\frac{\partial u}{\partial y}$$

$$q_L + \rho\ \overline{h'v'} = -\left(\frac{\mu}{P_r} + \frac{\rho\ e^{1/2}\ell}{P_{r_t}}\right)\frac{\partial h}{\partial y} \qquad (1)$$

The governing equations for e and ℓ are the turbulent kinetic energy equation and an equation for the rate-of-dissipation, $\varepsilon_d = C_d\ e^{3/2}/\ell$ where C_d is a constant.

The turbulence modeling equation for the turbulent kinetic energy has been used in various modern investigations, beginning with Bradshaw[4] and is reasonably well understood and accepted. Less certainty exists for the second turbulence modeling equation, and in fact, three types of equations have been proposed, and are:

1) Equations for the integral scale length, ℓ, as derived by Rotta[5] and Ng and Spalding[6].

2) Equations derived for the mean squared vorticity fluctuation, $\omega = e^{1/2}/\ell$, from the work of Saffman[7].

3) Equations for the dissipation rate of turbulent energy, $\varepsilon_d = C_d e^{3/2}/\ell$, from Harlow and Nakayama[8] and Jones and Launder[9].

Wilcox and Alber[10] found the integral scale length and vorticity fluctuation equations, and their respective universal constants, to be very similar in form and magnitude, respectively. For this reason, a comparative study was performed at TRW and reported in the ROPE Final Report[11] for 1972, just between the vorticity fluctuation and dissipation rate equations. It was found, for boundary layer flows, that the best agreement with experiment was achieved with the dissipation rate equation, and consequently, that is the equation applied here.

The form of these equations presently solved, written in streamfunction coordinates, is presented below:

Turbulent energy

(conv.) (prod.) (diss.) (comp.)

$$\frac{\rho U}{h_s}\frac{\partial e}{\partial s} = \mu_T (\rho u r^\alpha)^2 \left(\frac{\partial U}{\partial \psi}\right)^2 - \rho \varepsilon_d \left(1 + \frac{2}{C_d}\frac{1}{R_T}\frac{\ell^2}{n^2}\right) + \xi_1 \frac{e}{\gamma RT}\frac{U}{h_s}\frac{\partial P}{\partial S}$$

(diff.)

$$+ \frac{\rho U}{h_s}\frac{\partial}{\partial \psi}\left[(\mu + \sigma^* \mu_T)\, u r^{2\alpha} h_s \frac{\partial \rho e}{\partial \psi}\right] \qquad (2)$$

Turbulent dissipation rate ($\varepsilon_d = C_d e^{3/2}/\ell$)

(conv.) (prod.) (diss.)

$$\frac{\rho U}{h_s}\frac{\partial \varepsilon_d}{\partial s} = c_1 (\rho u r^\alpha)^2 \frac{\varepsilon_d}{e}\mu_T \left(\frac{\partial U}{\partial \psi}\right)^2 - \frac{\rho \varepsilon_d^2}{e}\left(c_2 + \frac{2}{C_d^2}\frac{1}{R_T}\frac{\ell^2}{n^2}\right) \qquad (3)$$

(comp.) (diff.)

$$+ \xi_2 \frac{\varepsilon_d}{\gamma RT}\frac{U}{h_s}\frac{\partial P}{\partial S} + \frac{\rho U}{h_s}\frac{\partial}{\partial \psi}\left[(\mu + \sigma \mu_T)\, \rho^{-\frac{1}{2}} u r^{2\alpha} h_s \frac{\partial \rho^{3/2} \varepsilon_d}{\partial \psi}\right]$$

where the turbulent viscosity is

$$\mu_T = \rho\, e^{1/2}\ell/(1 + 16.48/R_T)$$

and the turbulent Reynolds number is

$$R_T = \rho\, e^{1/2}\ell/\mu$$

The first term on the right-hand side of each equation is due to the production of turbulence by the working of the turbulent stress against the mean flow gradient. The second term on the right-hand side is due to the dissipation of turbulent energy and contains two parts. The first part is the dissipation rate as controlled by the macroscale, while the second part dominates at low R_T where the turbulence is in the microscale regime. As written, the latter term reflects the non-isotropy of the turbulence in the low R_T region of the boundary layer at the edge of the sublayer. This term has yet to be added to the wake formulation where, because the tendancy to isotropy in the microscale is much greater, it must be written in a form such as that presented by Finson[12].

The third term is due to compressibility and is a consequence of density-velocity correlations, and hence does not appear in incompressible flow. It was introduced by Wilcox and Alber who deduced the value of the constants ξ_1 and ξ_2 at about 2.5. These terms are very important during the expansion and subsequent recompression through the root of the wake shock, and from the results to be shown, it appears that these constants must be reevaluated; this will be discussed subsequently.

The forth term is the diffusion of turbulence by turbulence and, therefore, represents the triple correlations appearing in the fundamental form of the equations. The appearance of the density as ρe and $\rho^{3/2}\,\varepsilon_d$ in the derivative is a consequence of the earlier work on the compressible boundary layer. Two experimental observations for compressible turbulent flat plate flow are that the velocity profile under the Van Driest transformation $u^* = \int_0^u (\rho/\rho_e)^{1/2}\, du$, and the integral scale length, ℓ, are (within

the accuracy of the measurements) invarient with Mach number. Imposing these conditions on the turbulent energy and dissipation rate equations in the law-of-the-wall region suggested that the respective diffusion flux terms in the turbulent kinetic energy and dissipation rate equations should be $\frac{1}{\rho}\frac{\partial \rho e}{\partial y}$ and $\frac{1}{\rho^{3/2}}\frac{\partial\, \rho^{3/2}\, \varepsilon_d}{\partial y}$, respectively, to account for compressibility effects. This was confirmed in a calculation of Mach 5 adiabatic boundary layer and the results are shown in Figures 1, 2, and 3 where comparisons with the incompressible flow (Mach 0) flat plate results are made. In Figure 1, the agreement between the transformed velocity profiles is excellent in the law-of-the-wall and law-of-the-wake regions. The disagreement of the sublayer for $10 < y^* < 80$ may be due to the compressible scaling of the turbulent viscosity, μ_T, at low R_T, and further investigation to improve this region is underway. The proper invariance of the scale length, ℓ, with Mach number is demonstrated in Figure 2, and agreement with experiment is good. The trend with Mach number and the distributions of turbulent energy are also in good agreement with the data of Klebanoff[14] and Kistler[15] in Figure 3.

These compressibility corrections are assumed to be valid in the near wake, as well. However, calculations of the mixing layer have been initiated to provide an additional test of these corrections since a wealth of experimental data is available for this case.

From the left-hand side, it is seen that these four terms sum to yield the change in e and ε_d along streamlines. The equations contain several constants which are intended to be "universal", and are to be determined by comparison with experiment. This was done during the earlier boundary layer portion of the present task and is reported in the ROPE Final Report for 1972[11]. To summarize, they are listed below:

dissipation constant	$C_d = 0.09$
diffusion number for e	$\sigma^* = 1.0$
diffusion number for ε_d	$\sigma = .77$
production constant for ε_d	$c_1 = 1.41$
2nd dissipation constant for ε_d	$c_2 = 1.89$

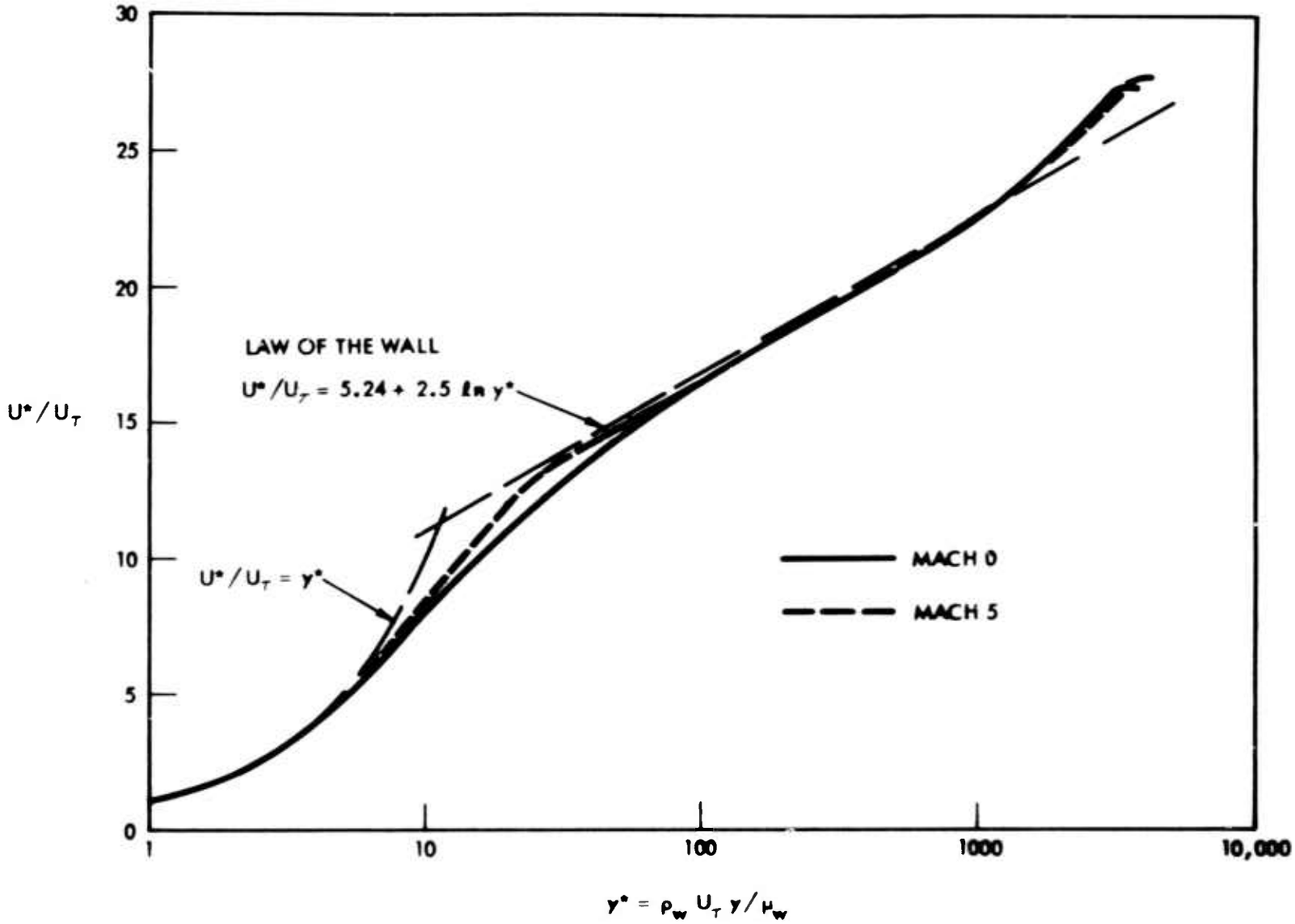

Figure 1. Turbulence Boundary Layer Calculation - Transformed Velocity Profiles for a Mach 0 and Mach 5 Adiabatic Flat Plate.

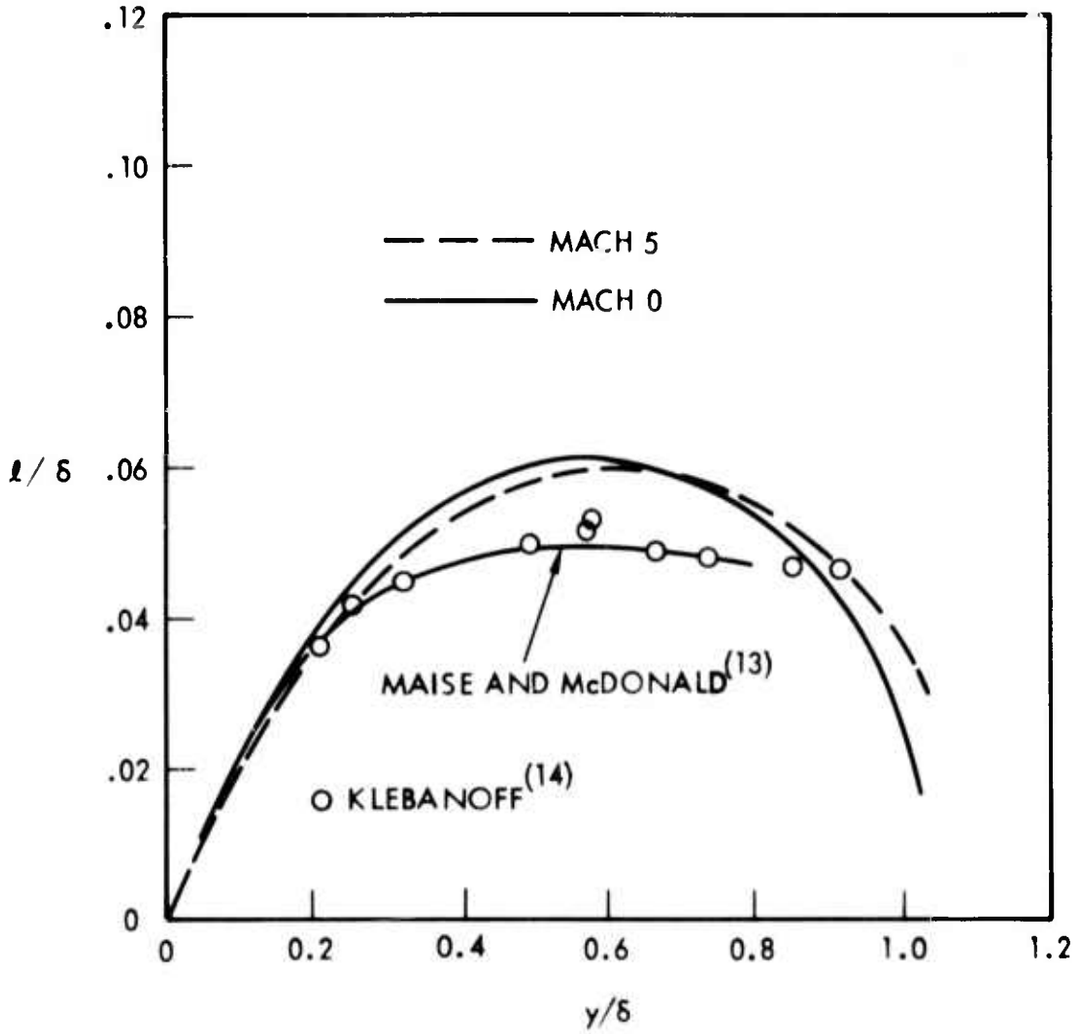

Figure 2. Turbulence Boundary Layer Calculation - Turbulent Scale Length

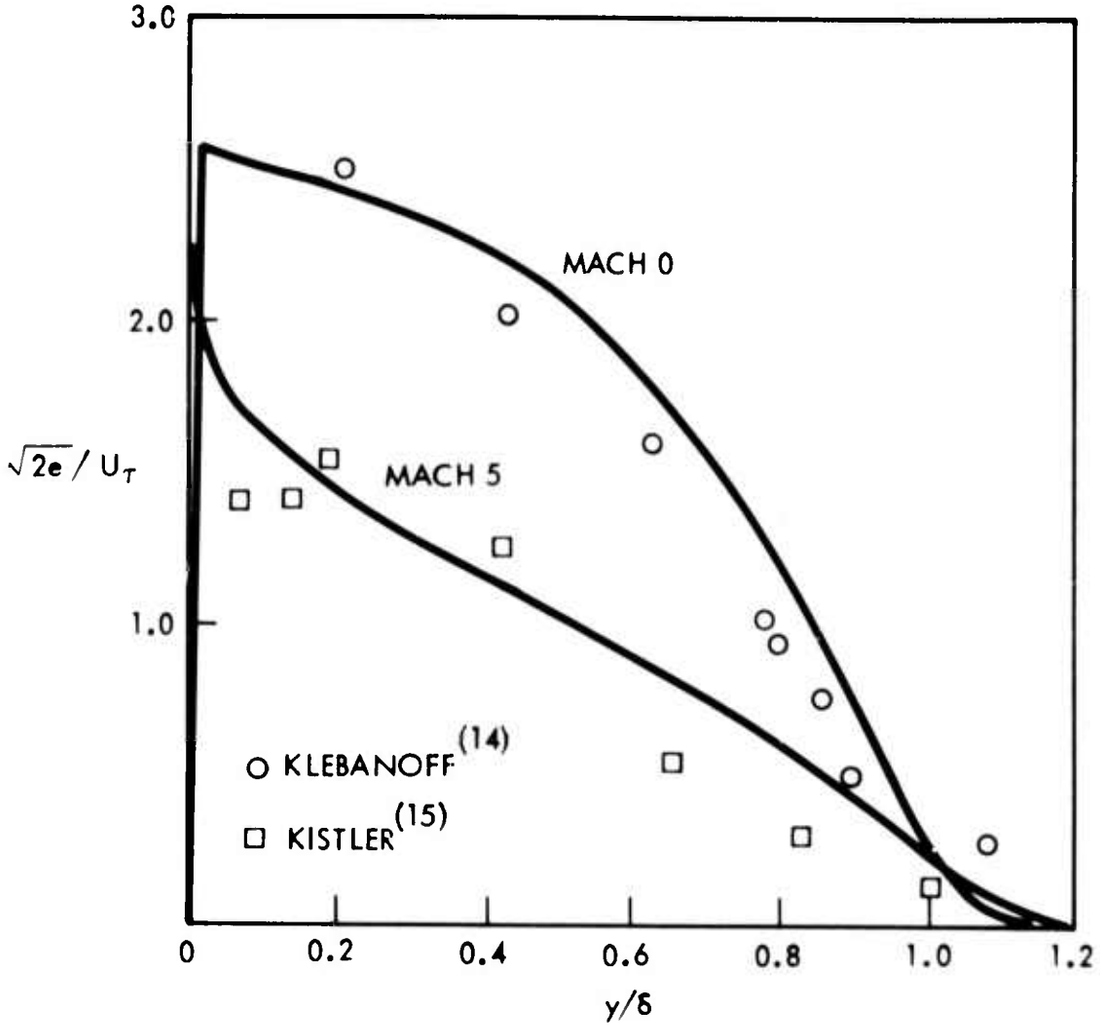

Figure 3. Turbulence Boundary Layer Calculation - Turbulent Kinetic Energy

compressibility constant for e	$\xi_1 = 2.5$
compressibility constant for ε_d	$\xi_2 = 2.5$

Equations 2 and 3 are seen to contain the mean flow variables and their cross-stream gradients, while the mean flow equations contain the turbulence variables through the flux terms of Equation 1. Thus, the mean flow and turbulence equations are mutually coupled and must be solved simultaneously at each point in the flowfield.

1.4 Division of the Wake into Two Regions

The recirculation region poses special problems in the near wake analysis because of the reverse flow region near the axis. Here, the parabolic governing equations are unstable to a marching calculation, which starts at the base and moves against the returning axis flow. This difficulty is circumvented by the application of an integral method which includes at least the entire recirculation region. Thus, as shown in Figure 4, the wake is divided into two regions about a "matching" streamline which lies adjacent to the dividing streamline. The inner region is solved by an integral method by marching downstream from the base simultaneously with the finite difference marching solution for the outer flow. A rigorous matching of essential flow properties is maintained on the matching streamline between the inner and outer regions at each step of the calculation.

In the integral analysis, the governing equations are integrated, radially, from the axis to the matching streamline ($r = \delta[x]$), yielding ordinary differential equations with the axial coordinate as the independent variable. These include the axial momentum, velocity moment of axial momentum, continuity, and energy equations. Profiles are assumed, and profile parameters are introduced such that additional auxiliary equations must be solved. These consist of the shear, heat transfer, and flow angle matches between the inner and outer regions, and a centerline energy equation. The integral region analysis applied here has been described in detail in References 2 and 3 for laminar flow. It is modified for turbulent flow according to Equation 1, and, in addition, the turbulence equations (Equations 2 and 3) are subjected to the integral formulation.

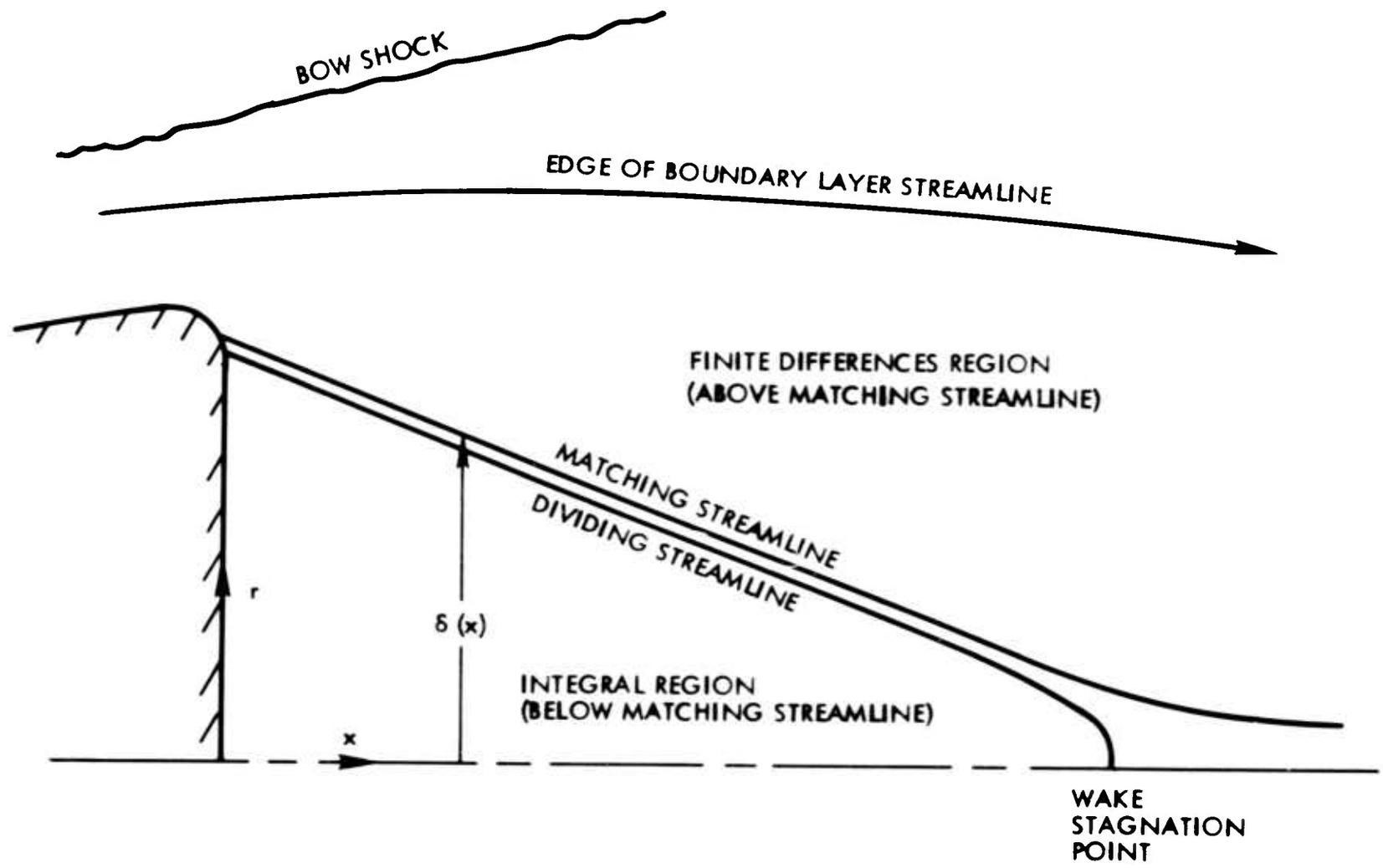

Figure 4. Two Region Near Wake Flow Model

The turbulence equations, in integral form, are:

Turbulent energy

$$\left.\begin{aligned} d(\rho_\delta\, u_\delta\, \delta^\lambda\, e_\delta\, I_{T_1})/dx = {} & \mu_T\, \delta^\lambda\, \Phi_\delta\, I_{T_2} - \delta^\lambda\, \rho_\delta\, \varepsilon_{d\delta}\, I_{T_3} \\ & + \xi_1\, \rho_\delta\, u_\delta\, \delta^\lambda\, e_\delta\, I_{T_1}\, dp/dx/(\gamma P) \\ & + (\mu + \sigma^* \mu_T)\, \delta^\alpha\, (\partial e/\partial r)_\delta \\ & + \sigma^* \mu_{T_\delta}\, e_\delta\, \delta^\alpha\, (\partial \rho/\partial r)_\delta\, \rho_\delta \end{aligned}\right\} \quad (4)$$

where $\Phi = (\partial u/\partial r)^2$, $\lambda = 1 + \alpha$ with $\alpha = 0$ or 1 for 2-dimensional or axisymmetric flow, respectively, and for $\eta = r/\delta$,

$$I_{T_1} = \int_0^1 \frac{\rho}{\rho_\delta} \frac{u}{u_\delta} \frac{e}{e_\delta}\, \eta^\alpha\, d\eta \quad (5)$$

$$I_{T_2} = \int_0^1 \frac{\mu_T}{\mu_{T_\delta}} \frac{\Phi}{\Phi_\delta}\, \eta^\alpha\, d\eta \quad (6)$$

$$I_{T_3} = \int_0^1 \frac{\rho}{\rho_\delta} \frac{\varepsilon_d}{\varepsilon_{d_\delta}}\, \eta^\alpha\, d\eta \quad (7)$$

Turbulent dissipation rate

$$\left.\begin{aligned} d(\rho_\delta\, u_\delta\, \delta^\lambda\, \varepsilon_{d\delta}\, I_{T_4})/dx = {} & c_1\, (\varepsilon'_{d\delta}\, e_\delta)\, \mu_{T\delta}\, \delta^\lambda\, \Phi_\delta\, I_{T_5} \\ & - c_2\, (\varepsilon'_{d\delta}/e_\delta)\, \delta^\lambda\, \rho_\delta\, \varepsilon_{d\delta}\, I_{T_6} \\ & + \xi_2\, \rho_\delta\, u_\delta\, \delta^\lambda\, \varepsilon'_{d\delta}\, I_{T_4}\, dp/dx/(\gamma P) \\ & + (\mu_\delta + \sigma \mu_{T\delta})\, \delta^\alpha\, (\partial \varepsilon'_d/\partial r)_\delta \\ & + 1.5\, \sigma\, \mu_{T\delta}\, \varepsilon'_{d\delta}\, \delta^\alpha\, (\partial \rho/\partial r)_\delta/\rho_\delta \end{aligned}\right\} \quad (8)$$

where $\varepsilon_d' = \varepsilon_d / C_d$ and

$$I_{T_4} = \int_0^1 \frac{\rho}{\rho_\delta} \frac{u}{u_\delta} \frac{\varepsilon_d}{\varepsilon_{d_\delta}} \eta^\alpha \, d\eta \tag{9}$$

$$I_{T_5} = \int_0^1 \frac{\mu_T}{\mu_{T_\delta}} \frac{\varepsilon_d}{\varepsilon_{d_\delta}} \left(\frac{e}{e_\delta}\right)^{-1} \frac{\Phi}{\Phi_\delta} \eta^\alpha \, d\eta \tag{10}$$

$$I_{T_6} = \int_0^1 \frac{\rho}{\rho_\delta} \left(\frac{\varepsilon_d}{\varepsilon_{d_\delta}}\right)^2 \left(\frac{e}{e_\delta}\right)^{-1} \eta^\alpha \, d\eta \tag{11}$$

The integrals are readily evaluated in closed form if profiles of the functions $\rho\Omega$ and μ_T are assumed where Ω has the units of vorticity (1/sec) and is related to e and ε_d by

$$\rho\Omega = \varepsilon_d / e \tag{12}$$

also,

$$\mu_T = \rho e^2 / \varepsilon_d \tag{13}$$

As in the integral analysis for the mean flow equations described in References 3 and 4, power low profiles are assumed of the form

$$\frac{\rho\Omega}{(\rho\Omega)_\delta} = E + (1 - E) \eta^\sigma \tag{14}$$

$$\frac{\mu_T}{\mu_{T_\delta}} = F + (1 - F) \eta^\sigma \tag{15}$$

where σ itself is a variable whose value, near the base, is very large (50 to 100), but then decreases away from the base reaching a value of 2 in the vicinity of the wake stagnation point. Thus, the growth of the mixing layer is characterized by the decrease in σ. The parameters, E

and F, appearing in Equations 14 and 15 represent axis values of $\rho\Omega$ and μ_T, respectively, in the integral region. Equations 4 and 8 are used to obtain the values of the turbulence variables e and ε_d at the matching streamline, and additional equations for the axis parameters E and F are required. The differential form of the turbulence equations, evaluated on the axis, would suffice for this purpose, but for the present, the axis values are simply equated to zero. This is acceptable in the recirculation region where the measurements of Lewis, et al[16] and Gran [1] have shown this region to be quiet of turbulence. However, the axis values can become significant downstream of the wake stagnation point due to the effects of turbulent diffusion, hence, the axis equations will be added in the very near future.

The integral region and outer finite differences region are rigorously coupled along the matching streamline at each interval of the calculation. The gradient terms appearing in Equations 4 and 8, namely, $(\partial e/\partial r)_\delta$, $(\partial \varepsilon_d'/\partial r)_\delta$, and $(\partial \rho/\partial r)_\delta$, are provided to the inner region from the outer flow. The inner region then supplies the outer flow with the four coefficients in the following linearization relations for iterations between the inner and outer regions,

$$de_\delta = \frac{\partial e_\delta}{\partial e_\psi} de_\psi + \frac{\partial e_\delta}{\partial \mu_{T\psi}} d\mu_{T\psi} \tag{16a}$$

and

$$d\mu_{T\delta} = \frac{\partial \mu_{T\delta}}{\partial e_\psi} de_\psi + \frac{\partial \mu_{T\delta}}{\partial \mu_{T\psi}} d\mu_{T\psi} \tag{16b}$$

where $e_\psi \equiv (\partial e/\partial \psi)_\delta$ and $\mu_{T\psi} \equiv (\partial \mu_T/\partial \psi)_\delta$. Equations 16 become the inner boundary conditions on the outer finite differences region above the recirculation region. When de_δ/e_δ and $d\mu_{T\delta}/\mu_{T\delta}$ are sufficiently small the solution is said to be converged for that step.

Details of the finite differencing scheme for the outer region equations are presented in References 2 and 3 and will not be repeated here.

1.5 Results

1.5.1 Mean Flow

First results have been obtained for a 6 degree half angle adiabatic cone at Mach 7.5 at $Re_{\infty D} = 1.7 \times 10^6$, corresponding to the wind tunnel experiment of Gran[1]. The solution was initiated on the straight portion of the cone, just upstream of the junction of the aft shoulder whose radius is 1/6 the base radius. Gran measured properties of the boundary layer here, and least-squares fit the following profile to the data,

$$\frac{U^*}{U_\tau} = \frac{1}{\kappa} \ell n \left(\frac{y\, U_\tau}{\nu_w} \right) + 5.0 + \frac{2\tilde{\pi}}{\kappa} \sin^2 \left(\frac{\pi y}{2\delta} \right) \qquad (17)$$

where U^* is defined by the Van Driest velocity transformation discussed earlier, and $\kappa = 0.41$. The profile was found to be very weak in the wake component with $\tilde{\pi} = 0.06$, instead of the usual 0.5. The other parameters are $U_\tau/U_e = .074$ and $\delta^* = \delta U_\tau/\nu_w = 142$ with $\delta/D = 0.044$. This profile and these parameters were used to initiate the present solutions.

Boundary layer separation profiles were generated on the shoulder for separation pressures in the range $0.15 \lesssim p_{sep.}/p_\infty \lesssim 0.26$. Subsequent wake solutions are shown in Figure 5, where the axis pressure and axis velocity are plotted as a function of the normalized distance from the base, X/D. As the base pressure is decreased, the character of the solutions is seen to change between solutions 3 and 4. For solutions 1, 2, and 3, the pressure continues to rise downstream of $X/D \tilde{=} 1$ while the axis velocity reaches a maximum and decreases to larger negative values. In fact, solutions 1 and 2 exhibit no positive velocity on the axis. However, solution 3 exhibits closure of the recirculation region, with a wake stagnation point at X/D = 1.2, followed by a redividing of the flow with a second wake stagnation point at $X/D \tilde{\sim} 1.25$. These solutions are referred to as source solutions where the inferred source acts on the axis in the direction of the base. Solutions 4 and 5 are sink solutions and are characterized by an axial pressure gradient which approaches minus infinity, and an axial velocity gradient which approaches plus infinity. These two non-wake-like

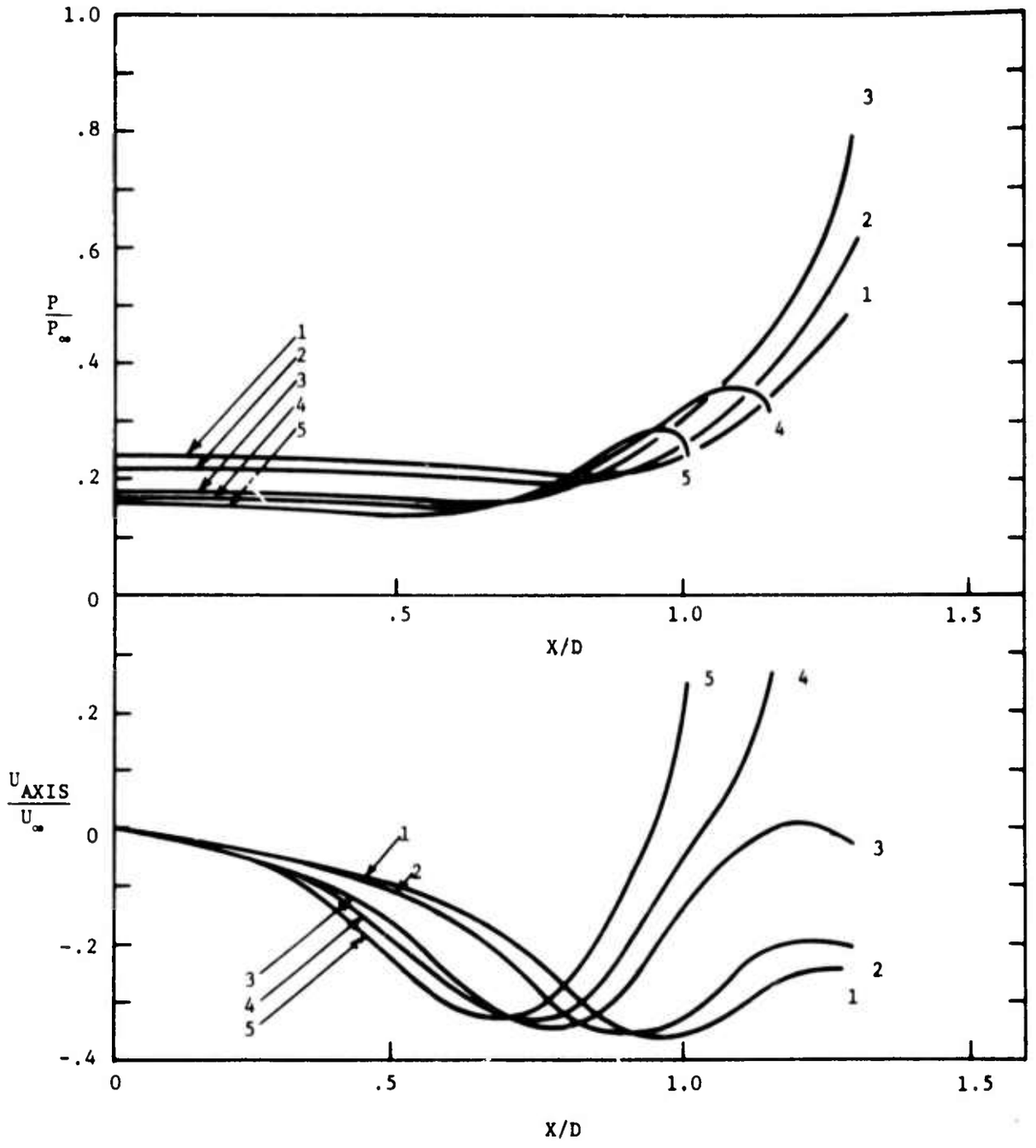

Figure 5. Turbulent Near Wake - Bracketing Solutions to the Wake Neck Singularity. $M_\infty = 7.5$, 6° cone, $Re_{\infty_D} = 1.7 \times 10^6$

families of solutions bracket the saddle point singularity in the wake neck. The singular solution of the saddle point is characterized by a single wake stagnation point and finite gradients of pressure and velocity. In the present case, the singular solution is bracketed by the separation solutions with separation pressures of $p_{sep}/p_\infty = .1659$ (sink) and $p_{sep}/P_\infty = .1785$ (source). This must be refined considerably for the analysis which carries the solution through the critical point. However, the present bracketing solutions are sufficiently close so that some comparisons with experiment can be made to ascertain whether further changes in the turbulence modeling are necessary.

The closest bracketing solutions are replotted in Figure 6, together with axis pressure data from Gran[1]. The solution is seen to lie below the measured value of $p_{base}/p_\infty = 0.24$. Also, the calculated pressure rise appears too steep to permit a smooth extrapolation into the data downstream of X/D = 2. Experience with laminar flow solutions suggests that the initial boundary layer profiles should be checked, since the base pressure has been found sensitive to the thickness and momentum deficite. Another important factor is the turbulence modeling and the resulting turbulent diffusivity approaching the wake neck. Turbulent shear acts to accelerate the flow through the strong adverse pressure gradient approaching the wake neck. Consequently, a modeling which produces excessive turbulence in the wake neck could cause an excessively large pressure gradient in this region. The turbulence approaching the wake neck will be examined later.

The streamline and shock wave patterns in the near wake are shown in Figure 7. The edge-of-boundary layer streamline is seen to have turned only slightly at the downstream extent of the calculation. Streamlines A through E are labeled for later reference. The curvature of the streamlines changes through the lip shock wave. The dividing streamline (DSL) is seen to intercept the axis at X/D $\tilde{\sim}$ 1.2. The asterisk denotes the matching streamline below which the integral analysis applies. The row of dots refers to the radial location where the turbulent viscosity is 50 percent of the local laminar viscosity. Upstream and above this locus, the flow is essentially laminar. The local maximum of the Pitot pressure delineates the wake shock. The lip shock is shown by the locus of minimum pressure along streamlines on the upstream side, and the locus of local maximum in Pitot pressure on the downstream side.

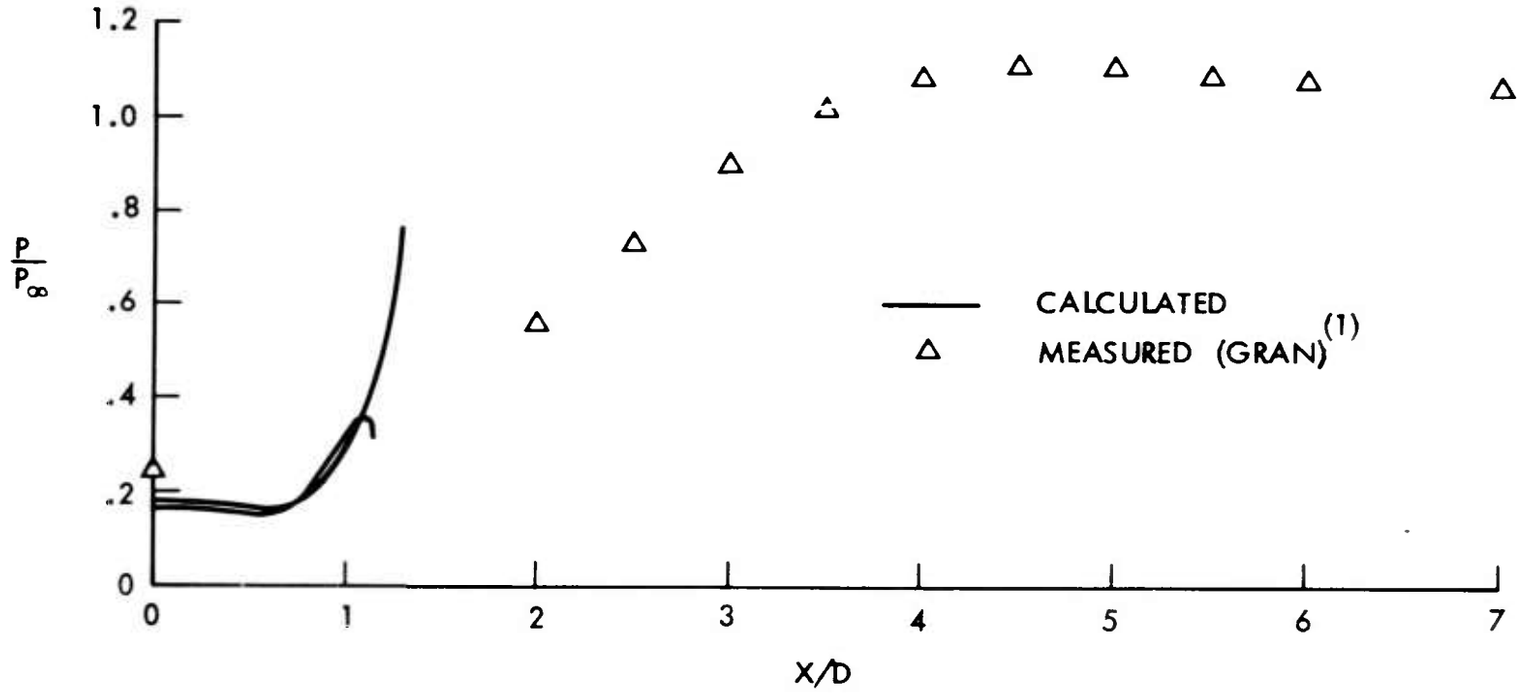

Figure 6. Turbulent Near Wake - Axis Pressure Comparison
$M_\infty = 7.5$, 6° cone, $Re_{\infty_D} = 1.7 \times 10^6$

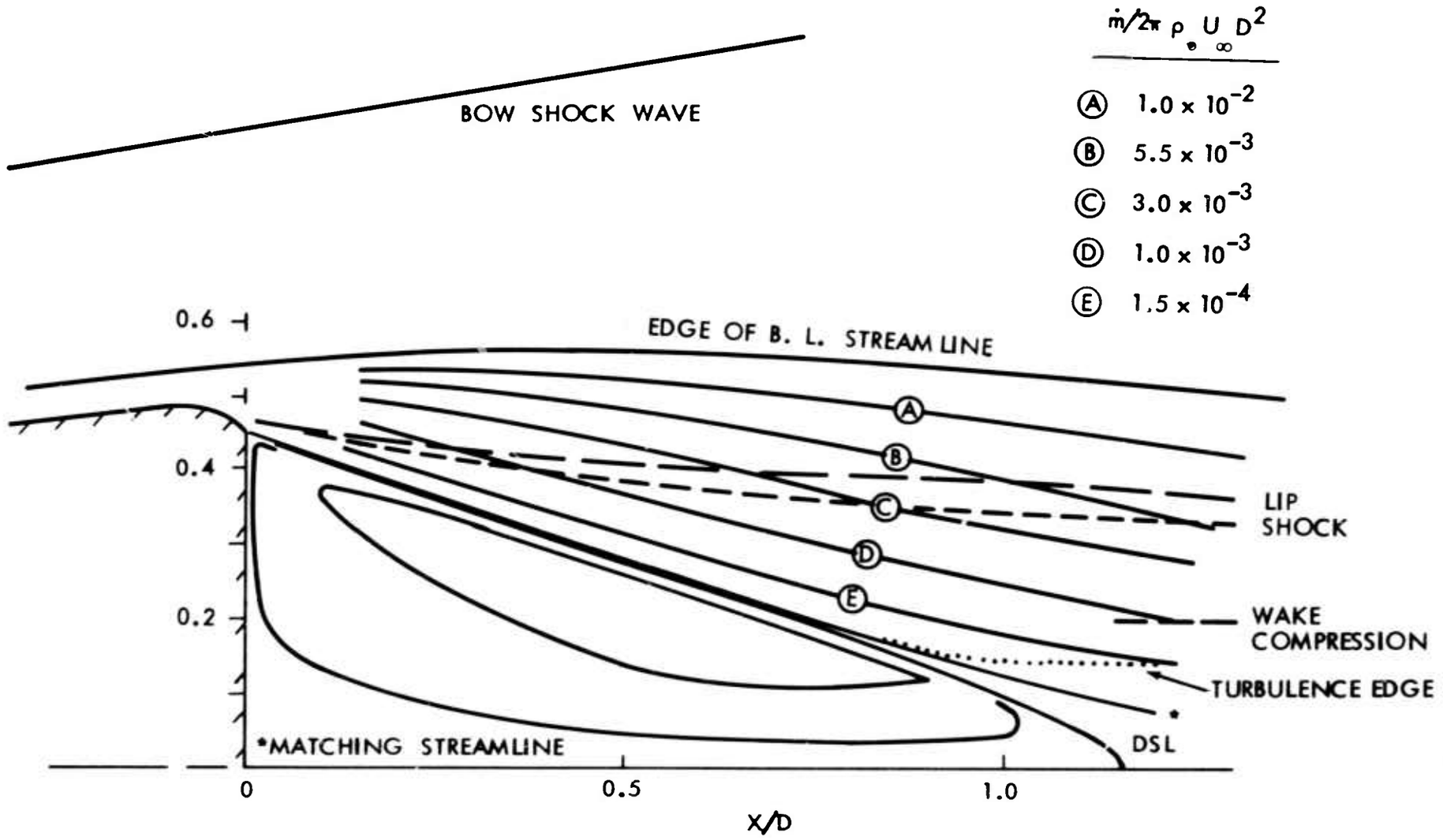

Figure 7. Turbulent Near Wake - Calculated Streamline and Shock Wave Patterns
M_∞ = 7.5, 6° cone, Re_{∞_D} = 1.7 x 10^6

The shock wave development is also easily seen in the pressure profile plot of Figure 8. The profile at X/D = 0 corresponds to separation with its origin on the shoulder. All the profiles are characterized by a strong decrease in pressure due to the expansion with a subsequent rise through the lip shock. The slight increase below the lip shock at X/D = 0.8 is due to early compressions which lead to the formation of the wake shock. A rather strong wake shock has developed at X/D = 1.2.

Velocity profiles are shown in Figure 9, and are relatively unperturbed by the shock waves. The growth of the mixing layer is evident as the profile broadens from X/D = 0 to X/D = 0.8. Since most of the flow is laminar, these results appear very similar to past laminar results.

1.5.2 Turbulent Properties

In the presentation of the turbulence equations, turbulence production was seen to depend on the square of the cross-stream velocity gradient. In Figure 9, the largest velocity gradients are present in the mixing layer and near axis wake just downstream of the wake stagnation point; consequently, these are the primary regions of turbulence production. However, in the results to be presented, the compressibility term containing the streamwise pressure gradient will dominate much of the growth and decay of turbulence in the near wake. The compressibility term behaves like a dissipation term in a favorable pressure gradient, $\partial p/\partial s < 0$, and a production term in an unfavorable pressure gradient, $\partial p/\partial s > 0$. With all other factors aside, it forces the turbulence to behave like a thermodynamic state property with a reversible character. In a balance just between the compressibility term and the convection term in Equations 2 and 3, the following simple relations emerge,

$$e \sim p^{\xi_1/\gamma} \tag{18}$$

$$\varepsilon_d \sim p^{\xi_2/\gamma} \tag{19}$$

These relations account for most of the turbulence decay during the expansion into the wake, and to the increase in turbulence across the lip and

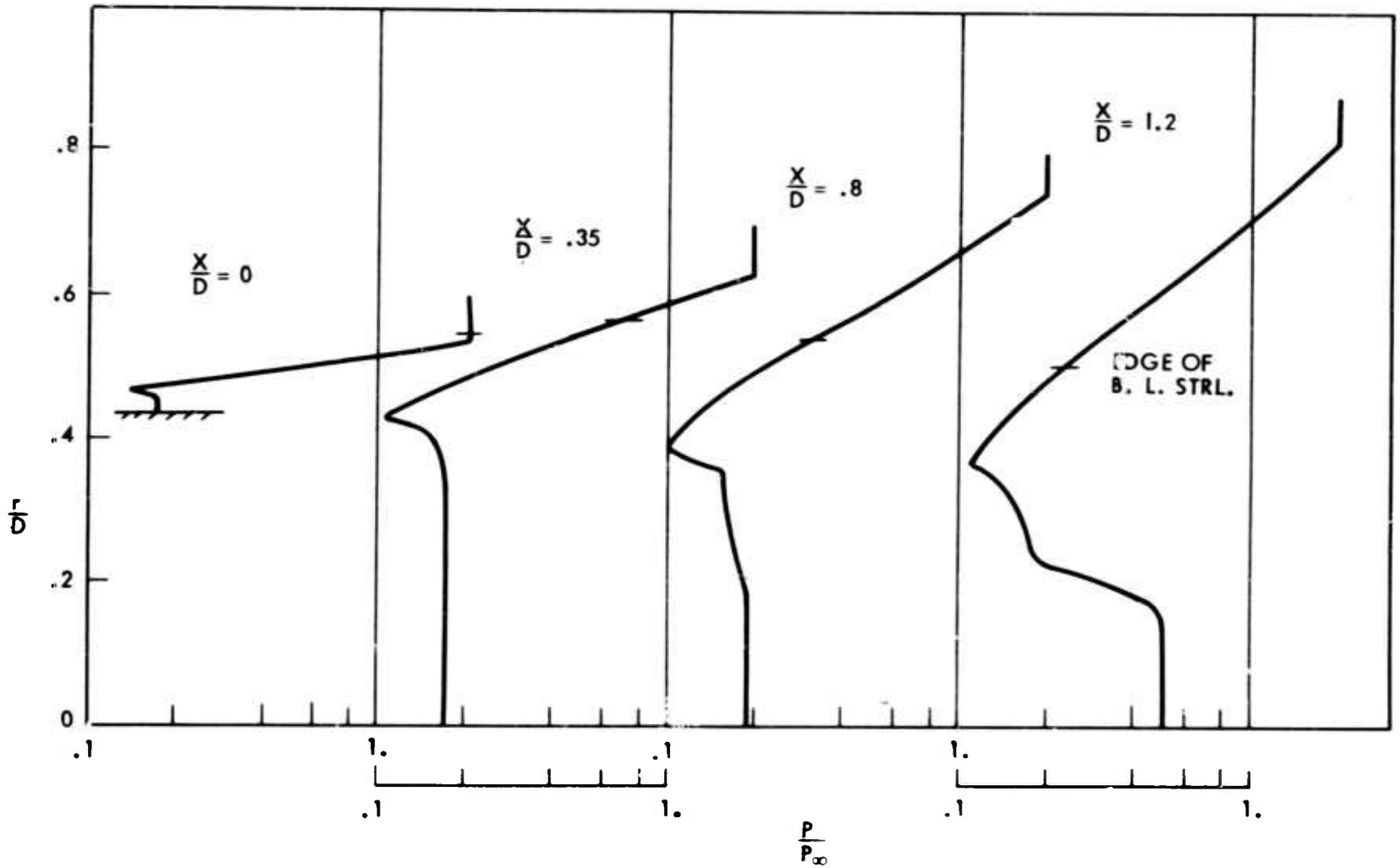

Figure 8. Turbulent Near Wake - Calculated Pressure Profiles
M_∞ = 7.5, 6° cone, Re_{∞_D} = 1.7 x 10^6

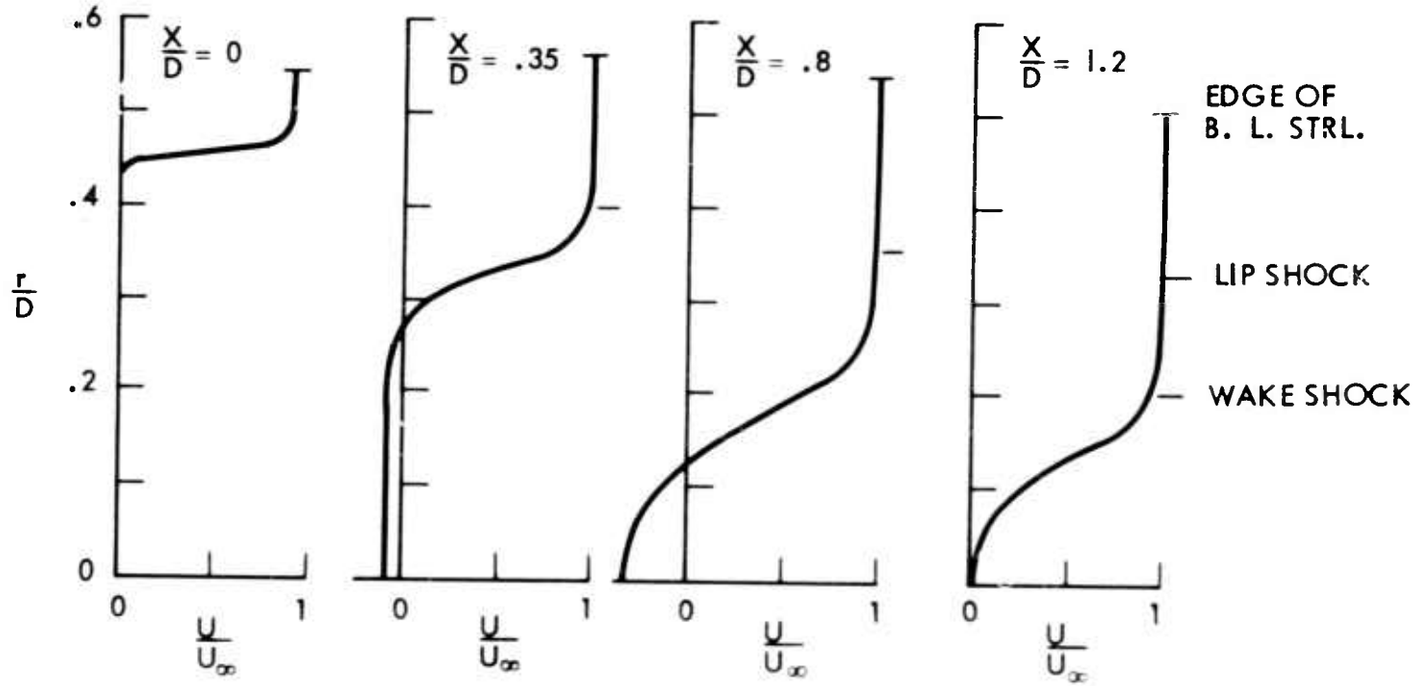

Figure 9. Turbulent Near Wake - Calculated Velocity Profiles
$M_\infty = 7.5$, 6° cone, $Re_{\infty_D} = 1.7 \times 10^6$

wake shock waves and in the region of rising axial pressure in the vicinity of the wake stagnation point. The effect may be seen in the profile plot of the turbulent kinetic energy, $e/U_\infty^2/2$, presented in Figure 10. The ordinate is the streamfunction, and the correspondence to the physical plane can be obtained from Figure 7. Curve 1 refers to the boundary layer on the cone upstream of the shoulder junction, while curve 2 refers to conditions at separation. The large decrease in energy between curves 1 and 2 is associated with the expansion. The outer regions of the boundary layer show less of a decrease because the flow here is subject to a smaller pressure drop due to the angle of propagation of expansion waves through the boundary layer. Curves 3 and 4 reflect the growth of the turbulent energy in the mixing layer in an essentially constant pressure region where the compressibility term is not important. Between curves 4 and 5, the flow undergoes a strong compression with a subsequent rapid rise in turbulent energy, largely due to the compressibility effect of Equation 18. The strong effect of compressibility on these results thus emerges, and the question arises as to their adherence to experimental data.

The data of Gran[1] does show a sharp decrease in turbulent energy in the expansive portion of the boundary layer remnant. Beginning with $e/U_\infty^2/2 \approx 4 \times 10^{-3}$ in the outer part of the boundary layer upstream of the shoulder junction, the measurements indicate a decrease to $e/U_\infty^2/2 \approx 1.5 \times 10^{-4}$ at $X/D > 0.5$. The present theoretical results show a decrease to less than $e/U_\infty^2/2 \approx 1. \times 10^{-5}$ for this same region with a corresponding pressure drop of 5 percent of the cone pressure. Consequently, it appears that the value of the constant, $\xi_1 = 2.5$, originally deduced by Wilcox and Alber[10] is too large and from calculations based on Equation 18, it is suggested that a value closer to unity would be more appropriate. Bradshaw[18] also recognized that the Wilcox-Alber value for ξ_1 was too large and suggested it be reduced to a number close to one.

Profiles of turbulent viscosity, normalized by the freestream laminar viscosity, are presented in Figure 11 with streamfunction as the ordinate. For the outermost streamlines, the expansion is seen to reduce the viscosity while retaining the idenity of the initial maximum in the boundary layer. Increases in the viscosity are noted as the streamlines pass through the lip and wake shock waves (curves 4 and 5 at $\dot{m}/2\pi \rho_\infty U_\infty D_\infty^2 > 5 \times 10^{-4}$) and

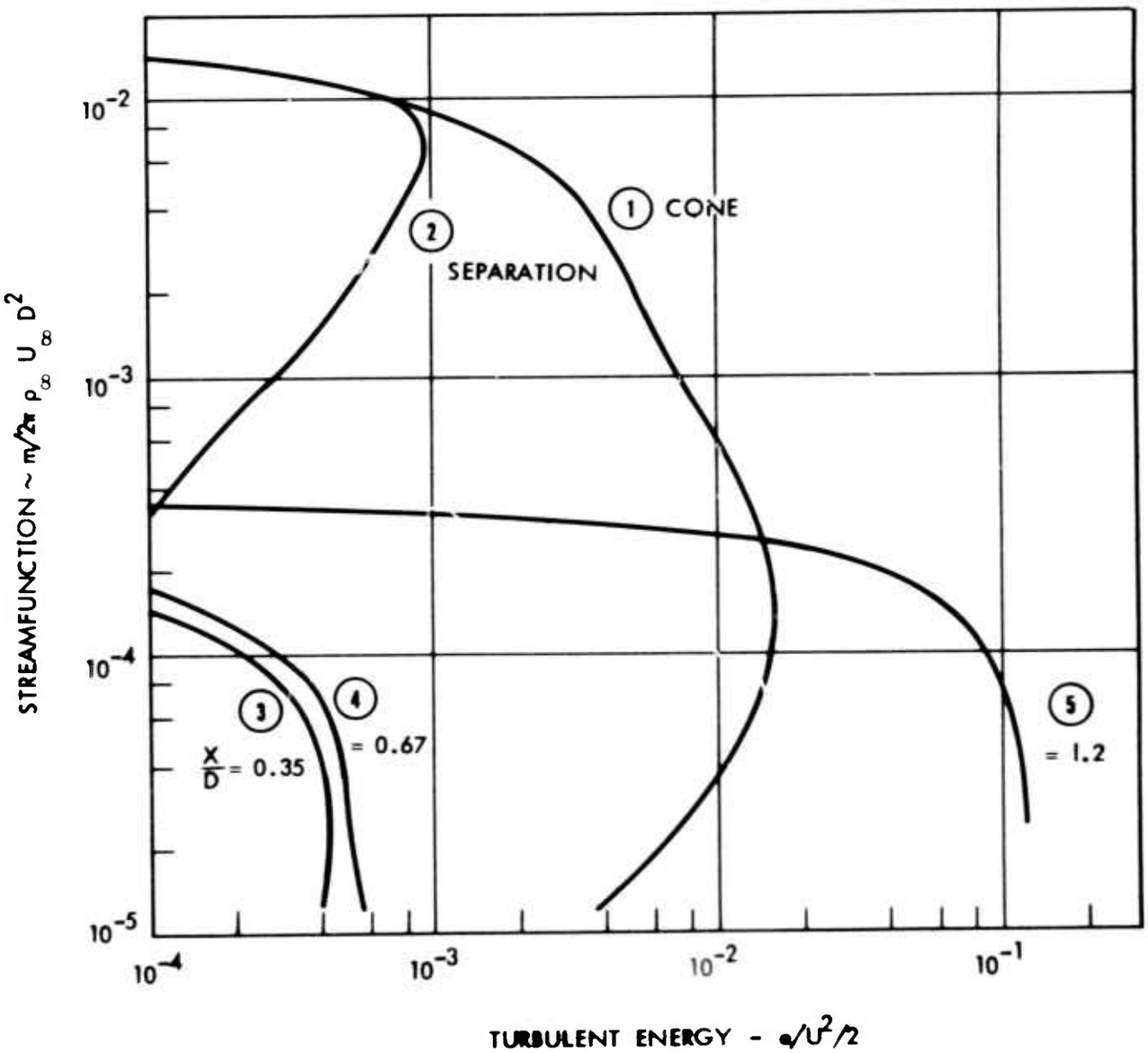

Figure 10. Turbulent Near Wake - Calculated Turbulent Energy
M_∞ = 7.5, 6° cone, $Re_{\infty D}$ = 1.7 x 10^6

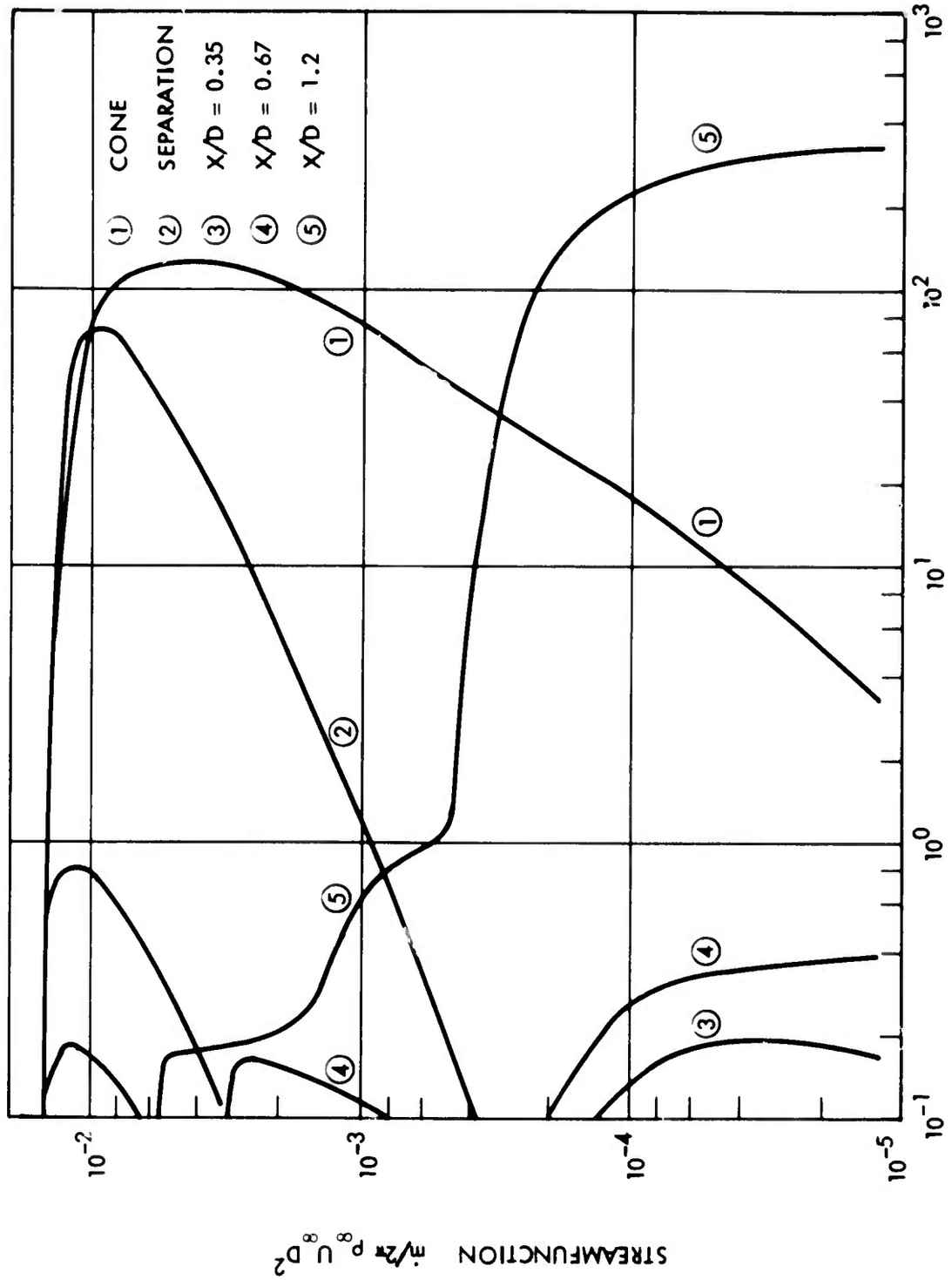

Figure 11. Turbulent Near Wake - Calculated Turbulent Viscosity
$M_\infty = 7.5$, 6° cone, $Re_{\infty_D} = 1.7 \times 10^6$

are due to the compressibility effect. The increase in viscosity on the innermost streamlines is due to turbulence production associated with the cross-stream velocity gradients in the mixing layer (curves 3 and 4), while the large increase between curves 4 and 5 is primarily the result of the compressibility term, i.e., to $\partial p/\partial s > 0$. In addition to the turbulent energy, compressibility is seen to dominate the behavior of the turbulent viscosity in much of the near wake flow, as well. Excluding all other effects except compressibility, the turbulent viscosity is approximately related to the pressure by

$$\mu_T = \rho e^{1/2} \ell = C_d \rho e^2/\varepsilon_d \sim p^{\frac{1}{\gamma}(1 + 2\xi_1 - \xi_2)} \tag{20}$$

If μ_T is to decrease during the expansion, then it follows that $2\xi_1 - \xi_2 > -1$. Furthermore, if from the earlier discussion, $\xi_1 = 1$, then $\xi_2 < 3$. A lower bound on ξ_2 can be found from consideration of the scale length, ℓ.

The data of Gran shows an increase in an integral scale length of the turbulence in the boundary layer remnant above the lip shock. Gran's scale length was derived from the autocorrelation function, and is not quantatively the same as the transverse scale length, ℓ, used in the present theory. However, the qualitative behavior should be approximately the same, i.e., a growth in the expansive portions of the flow is expected. In the expansion region along streamlines, the compressibility effect alone yields the following dependence upon pressure,

$$\ell = C_d e^{3/2}/\varepsilon_d \sim p^{(\frac{3}{2}\xi_1 - \xi_2)/\gamma} \tag{21}$$

In the present results, $\xi_1 = \xi_2 = 2.5$, and thus, the exponent is positive yielding a dependence on pressure which is opposite to that expected. To obtain a negative exponent, it is clear that $\xi_2 > \frac{3}{2}\xi_1$. For $\xi_1 = 1$, the bounds on ξ_2 are thus established as $1.5 < \xi_2 < 3$, and the presently assumed value of 2.5 thus lies within this range.

The effect of reducing the constant ξ_1 from 2.5 to 1.0 will reduce the decay of turbulence in the remnant and the subsequent growth in the

vicinity of the wake stagnation point. Because of the non-linear dependence on e and ℓ of the production and dissipation terms, it is difficult to know what the net effect on the solution will be. Clearly, the present calculations must be redone with a new value for ξ_1, and in addition, the low turbulence Reynolds number dissipation term of Finson's[12] model must be added.

1.6 Summary and Future Effort

The major problems encountered in the modification of the laminar near wake code to turbulent flow have been resolved, and a demonstration has been made to the ability of the code to generate solutions which bracket the wake neck singularity. The results have shown, for the various regions of the near base flow, the relative importance of the various terms in the turbulence modeling theory. Compressibility effects were found to be very strong, and comparisons with experiment indicated they were over-emphasized due to the use of an excessively large value for one of the compressibility constants; a more appropriate value was suggested from the data. Because the compressibility effect was so dominate in the present results, the Gran case must be recalculated with the new constant. The impact of this change on the mean flow is of particular interest, especially in the comparison of base pressure and axis pressure distribution with experiment.

A key question in the present analysis is whether all of the important effects which contribute to the growth and decay of turbulence in the near wake have been recognized, and if so, whether they have been properly characterized in the modeling. Because of the complex nature of turbulent flows, the answer will not come forth from analyses which start from first principles. Instead, the approach must involve hypothesis, experiment, and comparison. Fortunately, in the present problem, a number of experiments have been, and are being, performed with which the present theory can be applied and the results compared. In addition to the wind tunnel experiment of Gran[1], there are 1) the low Mach number high Reynolds number experiments of Demetriades at Philco-Ford, 2) the shock tube experiments of Holden at Calspan, 3) possible Ludweig tube experiments at Avco Rad, 4) ballistic range experiments at General Motors/Delco Division, and 5) the ballistic

range experiments at TRW by Fox*. These experiments span a wide range of conditions, and should in conjunction with the theoretical analysis lead to improvements in the modeling, as well as to an understanding of whether proper accounting has been made of the important effects. The latter should be established prior to application of the turbulent near wake code to the full reentry case.

*These experiments have been presented at the ABMDA-sponsored Wake Velocity Workshop held at General Motors/Delco Division in June 1973.

2. NEAR WAKE STABILITY STUDIES

2.1 Introduction

Observations of the wake velocity and turbulence spectral properties in the wake of hypersonic slender bodies have disclosed some dramatic changes after boundary layer transition, with evidence that two types of wake behavior occur. One is characterized by the generation of high amplitude fluctuations of relatively low frequency in the near wake, even in the presence of background residual turbulence from the boundary layer. This is accompanied by a rapid wake growth and followed by a broadening of the turbulence spectrum, evidence that the wake is dynamically unstable and undergoes a "transition" in the same way as does a laminar wake. A second type of behavior is observed which suggests that the wake, under other conditions, does not undergo these transitional processes. Both types of behavior can be observed within the range of conditions corresponding to the entry trajectory of a single vehicle, with a sudden change from the first type of behavior to the second with decending altitude.

The explanation of these phenomena appears to lie with the understanding of the stability properties of the near wake of slender hypersonic vehicles. In the ROPE Project Final Technical Report, November 1972,[11] a description of the results of a stability study of the wake of the RMV-340 at 39 km altitude was presented. The results, when compared with the full scale electrostatic probe measurements of Chang,[17] displayed remarkable agreement. The measurements correspond to an altitude at which boundary layer transition has just taken place at the rear of the body. The experimental observations include the detection of a predominant low frequency (300 Hz) fluctuation, a rapid increase in fluctuation amplitude in the near wake, followed by a decay in amplitude accompanied by a broadening of the turbulence spectrum. These observations are consistant with the existence of what would be termed, if the boundary layer were laminar, wake transition. Calculations of the amplification rates of linear disturbances were performed for corresponding conditions, and these yielded a sharply peaked amplification rate spectrum in the near wake, consistent in both frequency and axial location with the measurements. Subsequent calculations corresponding to

31 km altitude also yield agreement with the observations. However, in both cases, the calculated amplification rate of linear disturbances was quite small (with a characteristic length of $\sim$ 5 body diameters). For such small amplification rates to lead to transition within the near wake, sizable fluctuation amplitudes are required initially (with their origin within the body boundary layer or the shear layer bounding the base recirculation region). Amplification rates further downstream (after the boundary layer edge has crossed the wake shock) are predicted to be considerably smaller than in the near wake, so it is tempting to speculate that if a transitional process has not proceeded to the point that fluctuation amplitudes become large within the near wake, it will be delayed until far downstream.

Based on the small amplification rates predicted by these calculations, one would have to conclude that the major effects controlling transition in the near wake are those which determine the amplitude of fluctuations entering this region. There is, however, a possible source of fluctuations which has been neglected in the previous calculations and which should be examined before accepting such a conclusion. This is described in the following section.

2.2 Boundary Conditions for Fluctuation Equations

The partial differential equations, describing linear fluctuations in flow variables, are obtained from the conservation equations by expressing the variables in the form $u = \bar{u} + u'$, where prime denotes a perturbation. The conservation equations for the unperturbed variables are then subtracted and higher order perturbation terms neglected to obtain the linear fluctuation equations. These are reduced to ordinary differential equations by assuming a dependence on the independent variables of the form

$$u = \mathrm{Re}\left\{ U(r) \exp(i\theta) \right\} \quad \text{where } \theta = kx - \omega t + n\phi \tag{22}$$

Here, ω is real since we are interested in solutions periodic in time (no temporal amplification), and k is complex. The spatial amplification rate is k_i, and ϕ is the azimuthal angle.

In the near wake of a typical hypersonic slender body, the streamline originating at the edge of the body boundary layer does not cross the wake shock until $X/D \sim 6$. Between the wake stagnation point and a station far downstream of $X/D = 6$, then, the assumption that the wake is bounded by a semi-infinite uniform flow (as is done in boundary layer and far wake flows) is not valid. Boundary conditions are instead imposed at the wake shock by applying the condition that fluctuations cannot propagate outwards across the shock. Fluctuations just downstream of the shock are then associated with motion of the shock, and the flow just upstream of the shock is undisturbed. The boundary conditions are applied as follows:

Let $r = r_o(x) + Ae^{i\theta}$ be the shock location where $r_o(x)$ is the undisturbed shock location. The coefficient A is the (complex) amplitude of the perturbed shock. It follows that

$$\frac{\partial r}{\partial t} = - i\omega A e^{i\theta} \tag{23}$$

$$\frac{\partial r}{\partial x} = \frac{dr_o}{dx} + ik\, A e^{i\theta} \tag{24}$$

$$\frac{\partial r}{\partial \phi} = in\, A e^{i\theta} \tag{25}$$

$$\hat{n} = \frac{-\frac{\partial r}{\partial x}\hat{i} + \hat{j} - \frac{\partial r}{\partial \phi}\frac{\hat{k}}{r}}{\left[\left(\frac{\partial r}{\partial x}\right)^2 + 1 + \left(\frac{1}{r}\frac{\partial r}{\partial \phi}\right)^2\right]^{1/2}} \qquad \left(\begin{matrix}\text{unit vector}\\ \text{normal to shock}\end{matrix}\right) \tag{26}$$

$$\vec{V}_{\hat{n}} = \left(\frac{\partial r}{\partial t}\hat{j}\cdot\hat{n}\right)\hat{n} = \frac{\frac{\partial r}{\partial t}\hat{n}}{\left[\left(\frac{\partial r}{\partial x}\right)^2 + 1 + \left(\frac{1}{r}\frac{\partial r}{\partial \phi}\right)^2\right]^{1/2}} \qquad \left(\begin{matrix}\text{normal velocity}\\ \text{of shock}\end{matrix}\right) \tag{27}$$

If the velocity ahead of the shock is $u_1\hat{i} + v_1\hat{j}$, the normal (incoming) velocity with respect to the shock is

$$U_{1n} = \left[- u_1\hat{i} + \left(- v_1 + \frac{\partial r}{\partial t} \right) \hat{j} \right] \cdot \hat{n} \tag{28}$$

and the corresponding Mach number is

$$M_{1n} = \frac{U_{1r}}{a_1} \tag{29}$$

This Mach number is used to determine properties downstream of the shock including a fluctuating component (since M_{1n} has a fluctuating component). The fluctuations in M_{1n} are due to the changing orientation of the normal vector

$$\hat{n} = \frac{- \frac{dr_o}{dx}\hat{i} + \hat{j}}{\sqrt{\left(\frac{dr_o}{dx}\right)^2 + 1}} + \left\{ \frac{- k\hat{i} - k\frac{dr_o}{dx}\hat{j} - \frac{n}{r}\hat{k}}{\left[\left(\frac{dr_o}{dx}\right)^2 + 1\right]^{3/2}} \right\} iAe^{i\theta} \tag{30}$$

$$+ \cdots$$

and due to the radial velocity of the shock (the term $\frac{\partial r}{\partial t}\hat{j}$, or $-i\omega Ae^{i\theta}\hat{j}$). When there are radial gradients in the mean properties upstream of the shock, there is yet another source of fluctuations, since, then, u_1, v_1, and a_1 have fluctuating components in the shock-fixed coordinates (even though there are no fluctuating components in space-fixed coordinates). This is easily seen by expanding these non-fluctuating quantities in a series about the mean shock location, for instance

$$u_1 = \bar{u}_1 + \left(\frac{\partial \bar{u}}{\partial r}\right)_1 (r - r_o) + \cdots \tag{31}$$

Evaluating the expression at the instantaneous shock location gives the fluctuating component due to the motion of the shock through the gradient

$$u_1 = \bar{u}_1 + \left(\frac{\partial \bar{u}}{\partial r}\right)_1 Ae^{i\theta} + \cdots \tag{32}$$

There is, of course, a similar contribution obtained when the values at the downstream side of the shock ($\bar{u}_2 + u'_{2s}$ for instance) are converted from the shock-fixed frame of reference to a space-fixed frame of reference.

$$u'_2 = u'_{2s} - \left(\frac{\partial \bar{u}}{\partial r}\right)_2 Ae^{i\theta} \tag{33}$$

These mean-flow-gradient effects were not previously included in determining the fluctuation boundary conditions. Linear stability calculations incorporating these changes are in progress.

For conditions corresponding to the RMV-340 vehicle at 31 km altitude, results thus far indicate amplification rates which are substantially larger than those obtained from the earlier calculations. Figure 12 shows the axial variation of the amplification rate obtained for linear disturbance frequencies of both 105 Hz and 210 Hz for the first spiral mode (n = 1). It is interesting to note an important qualitative difference from previous calculations; the amplification rate at low frequencies appears to be weakly dependent on frequency up to a cut-off frequency at which the amplification rate very rapidly drops through zero. Higher frequencies are then damped. Preliminary results place the cut-off frequency in the range 210 → 320 Hz.

Once the body boundary layer edge has passed through the wake shock, the shock-driven amplification of low frequency disturbances ceases (X/D > 5.5 in Figure 12).

Calculations are continuing in order to obtain better resolution near the cut-off frequency and examine the effect of shock-driven amplification in the other azimuthal modes. The preliminary results, obtained thus far, are not inconsistent with the ideas previously presented, i.e., that there is a mechanism of amplification of disturbances which is unique to the near wake, and if this mechanism does not result in transition, a much more weakly amplifying (or perhaps damping) far wake can delay transition until far downstream.

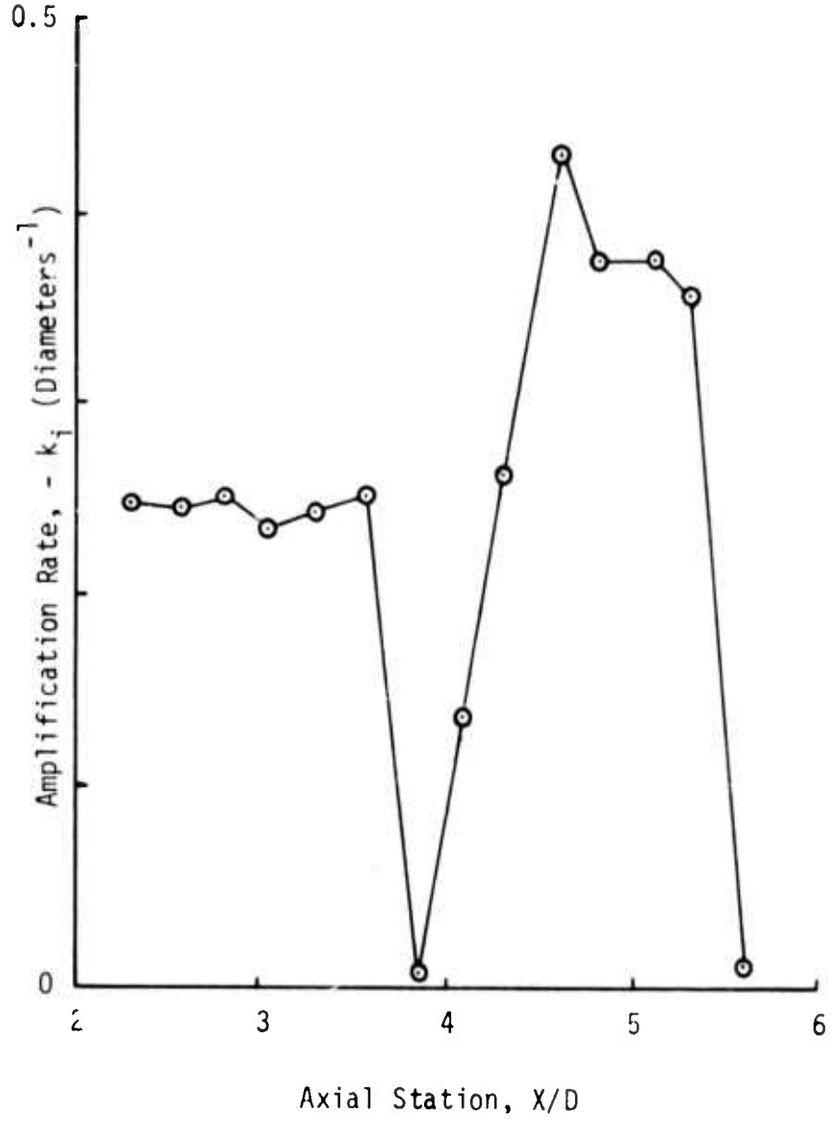

Figure 12. Amplification Rate of Linear Disturbances in the Near Wake of RMV-340 at 31 Km Altitude. Disturbance Frequency f = 105 Hz and 210 Hz (Results not Distinguishable on This Figure)

REFERENCES

1. Gran, R. L., "Reentry Observables Predictions and Experiments (ROPE), Final Report," TRW Report 18586-6035-RO-00, 28 July 1972.

2. Ohrenberger, J. T. and Baum, E., "A Theoretical Model of the Near Wake of a Slender Body in Supersonic Flow," AIAA Paper No. 70-792, Los Angeles, California, 1970.

3. Ohrenberger, J. T. and Baum, E., "A Theoretical Model of the Near Wake of a Slender Body in Supersonic Flow," AIAA Journal, Vol. 10, No. 9, pp. 1165-1172, September 1972.

4. Bradshaw, P., Ferriss, D. H., and Atwell, N. P., "Calculation of Boundary Layer Development Using the Turbulent Energy Equation," Journal Fluid Mech., Vol. 28, Part 3, pp. 593-616, 1967.

5. Rotta, J. C., "Statistiche Theorie nichthomogener Turbulenz 2 Mitt," Z Phys. 131, page 51, 1951.

6. Ng, K. H. and Spalding, D. B., "Predictions of Two-Dimensional Boundary Layer on Smooth Walls with a Two-Equation Model of Turbulence," Imperial College Report No. BL/TN/A/25, 1970.

7. Saffman, P. G., "A Model for Inhomogeneous Turbulent Flow," Proc. Roy. Soc. Lond. A, Vol. 317, pp. 417-433, 1970.

8. Harlow, F. H. and Nakayama, P. I., "Turbulent Transport Equations," Physics of Fluids 10, No. 11, pp. 2323-2332, 1967.

9. Jones, W. P. and Launder, B. E., "The Prediction of Laminarization with a Two-Equation Model of Turbulence," Int. Journal Heat Mass Transfer, Vol. 15, pp. 301-314.

10. Wilcox, D. C. and Alber, I. E., "A Turbulence Model for High Speed Flows," Heat Transfer and Fluid Mechanics Institute Proceedings, June 1972.

11. "ROPE Project Final Technical Report, Volume II - Reentry Observables," TRW Report 18586-6047-RO-00, 28 November 1972.

12. Finson, M. L., "Hypersonic Wake Aerodynamics at High Reynolds Numbers," AIAA Paper No. 72-701, June 1972.

13. Maise, G. and McDonald, H., "Mixing Length and Kinematic Eddy Viscosity in a Compressible Boundary Layer," AIAA Paper No. 67-199, Presented at AIAA 5th Aerospace Sciences Meeting, 1967.

14. Klebanoff, P. S., "Characteristics of Turbulence in a Boundary Layer with Zero Pressure Gradient," NACA TN 3172, 1954.

REFERENCES (Continued)

15. Kistler, A. L., "Fluctuation Measurements in a Supersonic Turbulent Boundary Layer," Physics of Fluids, Vol. 2, No. 3, pp. 290-296, 1959.

16. Lewis, J. E. and Behrens, W., "Fluctuation Measurements in the Near Wake of a Wedge with and without Base Injection," AIAA Journal, Vol. 7, No. 4, pp. 664-670, 1969.

17. Chang, J. H., "Full-Scale Wake Transition Measurements," AIAA Paper No. 73-109, Washington D.C., January 1973.

18. Bradshaw, P., "Anomalous Effects of Pressure Gradient on Supersonic Turbulent Boundary Layers," Imperial College Aero Report 72-21, November 1972.